frontiers | Frontiers in Energy Research

TYPE Original Research
PUBLISHED 23 February 2023
DOI 10.3389/fenrg.2023.1148734

OPEN ACCESS

EDITED BY
Sayed Abulanwar,
Mansoura University, Egypt

REVIEWED BY
Abdelhady Ghanem,
Mansoura University, Egypt
Dejian Yang,
Northeast Electric Power University, China

*CORRESPONDENCE
Heling Dong,
435709576@qq.com

SPECIALTY SECTION
This article was submitted to Process and Energy Systems Engineering, a section of the journal Frontiers in Energy Research

RECEIVED 20 January 2023
ACCEPTED 15 February 2023
PUBLISHED 23 February 2023

CITATION
Dong H, Tang Z and Wei M (2023), Two-stage robust optimal operation of AC/DC distribution networks with power electronic transformers.
Front. Energy Res. 11:1148734.
doi: 10.3389/fenrg.2023.1148734

Two-stage robust optimal operation of AC/DC distribution networks with power electronic transformers

Heling Dong*, Zhong Tang and Minjie Wei

School of Electric Power Engineering, Shanghai University of Electric Power, Shanghai, China

Power electronic transformers (PET) are a new type of power electronic equipment with a multi-port flexible dispatch function, which can play the role of a power hub in a system composed of multiple AC-DC hybrid distribution grids for interactive sharing of power in multiple regions. In this study, a two-stage robust optimization operation model of a hybrid AC-DC distribution network with PET is proposed based on PET power transmission and transformation characteristics. The stochastic uncertainty of the distributed renewable energy output in the AC-DC grid is handled by a two-stage robust optimization method to determine the minimum total system operation cost under the worst case of distributed renewable energy output. Finally, a constrained column generation algorithm is used to solve the two-stage robust optimization model in the min-max-min form and verifies the validity of the model in this study.

KEYWORDS

optimal dispatching, power electronic transformer, AC/DC distribution network, two-stage robust optimization, renewable energy, distributed generation

1 Introduction

With the development of power technology, new energy sources represented by wind and photoelectricity are increasingly connected to power systems and generally belong to distributed generation (DG). The DC part of the AC/DC mixed current distribution is compatible with these DGs, and DC transmission can reduce the number of energy conversions and improve energy utilization, while the AC part is compatible with existing power equipment, saving costs. The AC-DC hybrid distribution grid also has advantages in terms of new energy consumption, peak shaving, and valley filling, and is a feasible solution to cope with future grid development.

A power electronic transformer (PET) consists of a power electronic converter and conventional high-frequency transformer, which allows for more flexible conversion of electrical energy through power electronics technology (Liu et al., 2017; Wang et al., 2017). Generally, power electronic transformers are classified into AC/AC- and AC/DC/AC-type PETs, depending on whether they contain a DC component (Li et al., 2018). PET plays the same role as a traditional voltage source converter (VSC) in an AC/DC distribution network, connecting the AC and DC components of the interactive distribution network. Compared with traditional VSC, PET has some unique advantages, such as its ability to contain multiple AC-DC converter ports, connect multiple AC and DC subgrids simultaneously, control the power and voltage of each port, and achieve power quality control, fault isolation, and energy interaction between ports

simultaneously. Therefore, PET can play the role of an energy hub in the AC-DC hybrid distribution network.

Pu et al. (2018) provided an overview of the technology and framework for the optimal operation of PET-based hybrid AC-DC systems, and illustrated the advantages of PET-based AC-DC distribution networks over other power conversion units, such as VSC-based AC-DC distribution networks. Yi and Wang, 2021 proposed a day-ahead economic operation strategy for multi-port PET-based AC-DC distribution networks, reflecting the flexible regulation capability of PET, and established a PET energy flow model. Guo et al. (2019) applied multi-port PET to AC-DC hybrid distributed energy systems, fully consuming renewable energy and reducing system operation cost by using the power regulation function of PET. However, most of the above models do not fully consider the uncertainty of the renewable energy power output, whose random uncertainty significantly affects the power interaction of PET and safe operation of the AC-DC distribution network with access to large-scale scenic power sources.

Owing to the access of a large number of distributed renewable energy sources such as photovoltaic (PV) and wind power, the power supply of the grid has more uncertainty and volatility, posing new challenges for optimal dispatching of the distribution network. The commonly used uncertainty optimization methods include stochastic and robust optimization.

The probability distribution of random variables must be set in stochastic optimization, but the assumed probability distribution model may not be able to accurately portray the variation pattern of the actual uncertainty factors when they are more complex. Zhang et al. (2022) proposed a stochastic optimization model for the impact of new energy uncertainty on the operation results of AC-DC distribution networks containing power electronic transformers. Xu et al. (2021) combined stochastic optimization and conditional value-at-risk theory to propose a stochastic operation optimization method for active distribution networks containing smart soft switches considering risk management. Robust optimization does not require prior knowledge of the specific probabilistic prediction information of uncertain quantities and uses uncertainty sets to model uncertainty and pursue the minimum total cost of system decision options under the worst-case scenario with uncertain variables. Liu et al. (2018) considered the uncertainty of new energy and load, developed a min-max-min two-stage robust optimization model, and regulated the model conservativeness by introducing uncertainty regulation parameters. Fu et al. (2019) proposed a reactive voltage control method for AC-DC distribution networks based on a two-stage robust optimization model and examined the results of the model under different prediction errors. Liao et al., 2020 proposed a two-stage robust optimization strategy for an AC-DC distribution network with an optical storage consortium and used a hierarchical approach to set two objectives to solve it. Zhang et al. (2022) proposed a two-stage robust optimization model incorporating both distribution network reconfiguration and reactive power optimization. Zhong et al. (2022) introduced game theory into the two-stage robust optimization model for AC-DC distribution networks and constructed a master-slave game optimization model. However, few of the above models apply the two-stage robust optimization method to the optimal operation of hybrid AC-DC distribution networks with PET, and further research is required to combine the robust modeling idea with the optimal operation of AC-DC distribution networks with PET.

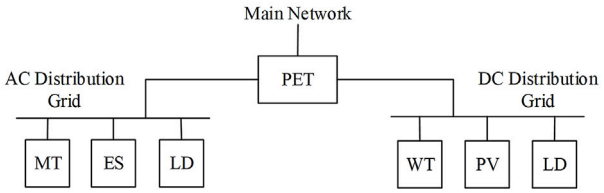

FIGURE 1
Schematic diagram of AC/DC distribution network with PET.

In this study, a two-stage robust optimal operation model of a hybrid AC-DC distribution network with PET is proposed. By connecting the AC-DC part of the distribution network and the super grid through PET, the utilization rate of distributed renewable energy is improved, and the safe and economic operation of the AC-DC distribution network is ensured. A two-stage robust optimization method is used to address the stochastic uncertainty of the renewable energy output and seek the minimum total system operation cost under the worst case scenario. Finally, a constrained column generation algorithm is used to solve the two-stage optimization model in the form of min-max-min.

Compared with the examples mentioned in the previous section, the two-stage robust optimization method used in this paper has the following advantages: first, compared with the traditional robust optimization method and the stochastic optimization method, the method used in this paper inherits the advantages of robust optimization such as strong accuracy and low out-of-bounds rate, and achieves the purpose of controlling the conservativeness of the model by adding uncertainty adjustment parameters. Secondly, compared with other two-stage robust optimization methods, the method used in this paper sets both spatial and temporal uncertainty adjustment parameters, which can control the number of bad scenarios taken in one cycle and the number of bad scenarios taken at the same time respectively, so that the conservativeness of the model can be controlled more flexibly and accurately to achieve better optimization results.

2 Two-stage robust operation model of AC/DC distribution network with power electronic transformers

2.1 Hybrid AC/DC distribution network structure with power electronic transformers

The hybrid AC-DC distribution network can be divided into three parts according to its composition: AC and DC distribution networks and VSC. The model in this paper used PET to replace the traditional VSC, which connects the DC, AC, and super grids and plays the role of power conversion. In the AC part, the micro turbine (MT), AC load, and energy storage (ES) are connected, and in the DC part, the PV, wind turbine (WT), DC load, and other parts are connected. The AC and DC parts are connected to the superior grid through PET. Figure 1 shows a schematic of the AC-DC hybrid distribution network. Compared with the traditional AC-DC distribution network, that with PET can directly

interact with the superior grid through PET, owing to the multi-port nature of PET, avoiding the loss caused by the interaction through the AC grid. Because the power can be freely interacted with in three ports, it improves the flexibility of power dispatching in the distribution network. Compared with traditional VSC, it improves the response speed and network flexibility and reduces the power conversion link, which is more suitable for distribution networks with uncertain DG (Pu et al., 2018; Li et al., 2021).

2.2 Equations

The optimization objective was to minimize the total operating cost during the dispatch cycle of the system. This entailed finding the operating solution with the lowest cost during the dispatch cycle by adjusting the purchased power from the higher grid, generation capacity of the micro turbine, and power of the energy storage equipment.

$$\min f = C^{M} + C^{MT} + C^{ES} + C^{PV} + C^{WT} \tag{1}$$

Among them,

$$C^{M} = \sum_{t\in T} c_t^{M} P_t^{M} \Delta t \tag{2}$$

$$C^{MT} = \sum_{t\in T} \sum_{i\in B^{MT}} \left(c_1^{MT} \left(P_{i,t}^{MT}\right)^2 + c_2^{MT} P_{i,t}^{MT} + c_3^{MT} \right) \Delta t \tag{3}$$

$$C^{ES} = \sum_{i\in B^{ES}} \sum_{t\in T} \left(c^{ES} (\eta P_{i,t}^{ch} - \frac{P_{i,t}^{dis}}{\eta}) \right) \Delta t \tag{4}$$

$$C^{WT} = \sum_{i\in B^{WT}} \sum_{t\in T} \left(c^{WT} (\tilde{P}_{i,t}^{WT} - P_{i,t}^{WT}) \right) \Delta t \tag{5}$$

$$C^{PV} = \sum_{i\in B^{PV}} \sum_{t\in T} \left(c^{PV} (\tilde{P}_{i,t}^{PV} - P_{i,t}^{PV}) \right) \Delta t \tag{6}$$

where f is the operation cost of the distribution network; C^{M} and C^{MT} are the costs of electricity purchased from the upper grid and generated by micro turbines, respectively; C^{ES} is the cost of energy storage; and C^{WT} and C^{PV} are the costs of abandoned wind and light, respectively. T is the operating period; B^{MT}, B^{ES}, B^{WT}, and B^{PV} are the sets of micro turbine nodes in the distribution network, energy storage nodes, wind turbine nodes, and photovoltaic nodes. c_t^{M} is the price of electricity purchased from the superior grid at time t; P_t^{M} is the power purchased from the superior grid by the distribution grid; and c_1^{MT}, c_2^{MT}, c_3^{MT} are the cost coefficients of micro turbine generation. $P_{i,t}^{MT}$ is the power output of micro turbine at node i at time t; c^{ES} is the cost coefficient of energy storage charging and discharging; η is the charging and discharging efficiency; $P_{i,t}^{ch}$ is the charging power of energy storage node i at time t; and $P_{i,t}^{dis}$ is the discharging power of energy storage node i at time t. C^{WT} and C^{PV} are the wind and light abandonment penalty coefficients, respectively; $\tilde{P}_{i,t}^{WT}$ and $\tilde{P}_{i,t}^{PV}$ are the predicted values of scenic output; and $P_{i,t}^{WT}$ and $\tilde{P}_{i,t}^{PV}$ are the actual scenic output values.

2.3 Constraints

2.3.1 Constraints of DistFlow branch currents in AC-DC distribution networks

The DistFlow tidal model was planned to be used for both the AC and DC parts of this model because part of this model contained non-linear terms that were not favorable for solving the model using software. To improve the solution speed, in this study, linearization and second-order cone relaxation were used to transform the model into a linear problem (Lavaei and Low, 2012), which was then solved by a commercial solver to achieve an easy solution and increase the solution speed as follows:

First, linearization transformation was performed through variable substitution:

$$\begin{cases} \left(V_i^{AC}\right)^2 = \tilde{V}_i^{AC} \\ \left(I_i^{AC}\right)^2 = \tilde{I}_i^{AC} \\ \left(V_i^{DC}\right)^2 = \tilde{V}_i^{DC} \\ \left(I_i^{DC}\right)^2 = \tilde{I}_i^{DC} \end{cases} \tag{7}$$

The results of the second-order cone relaxation of the DistFlow power flow model of the AC/DC hybrid distribution network were as follows.

AC part:

$$P_{j,t}^{AC} = \sum_{k\in\delta(j)} P_{jk,t}^{AC} - \sum_{i\in\pi(j)} \left(P_{ij,t}^{AC} + \tilde{I}_{ij,t}^{AC} r_{ij} \right) \tag{8}$$

$$Q_{j,t}^{AC} = \sum_{k\in\delta(j)} Q_{jk,t}^{AC} - \sum_{i\in\pi(j)} \left(Q_{ij,t}^{AC} + \tilde{I}_{ij,t}^{AC} x_{ij} \right) + b_i \tilde{V}_{i,t}^{AC} \tag{9}$$

$$\tilde{V}_{j,t}^{AC} = \tilde{V}_{i,t}^{AC} - 2\left(r_{ij} P_{ij,t}^{AC} + x_{ij} Q_{ij,t}^{AC} \right) + \left(r_{ij}^2 + x_{ij}^2 \right) \tilde{I}_{ij,t}^{AC} \tag{10}$$

$$\left\| \begin{matrix} 2P_{ij,t}^{AC} \\ 2Q_{ij,t}^{AC} \\ \tilde{I}_{ij,t}^{AC} - \tilde{V}_{j,t}^{AC} \end{matrix} \right\|_2 \le \tilde{I}_{ij,t}^{AC} - \tilde{V}_{j,t}^{AC}, \forall t \tag{11}$$

$$P_{j,t}^{AC} = P_{j,t}^{MT} + P_{j,t}^{ch} + P_{in,t}^{ACPET} - P_{out,t}^{ACPET} - P_{j,t}^{dis} - P_{j,t}^{ACLoad} \tag{12}$$

$$Q_{j,t}^{AC} = Q_{j,t}^{MT} + Q_{in,t}^{ACPET} - Q_{out,t}^{ACPET} - Q_{j,t}^{ACLoad} \tag{13}$$

where $\delta(j)$ is the set of end nodes with j as the first node, $\pi(j)$ is the set of first nodes with j as the end node, B^{AC} is the set of AC subnetwork nodes, and L^{AC} is the set of AC subnetwork branches. $P_{ij,t}^{AC}$, $Q_{ij,t}^{AC}$ are the active and reactive power flowing from node i to node j in the AC subnetwork, respectively; r_{ij}, x_{ij}, and b_i are the resistance and reactance of the branch ij and the shunt electrons at node i, while $P_{j,t}^{AC}$, $Q_{j,t}^{AC}$, $\tilde{V}_{t,j}^{AC}$, and $\tilde{I}_{ij,t}^{AC}$ are the active power, reactive power, voltage squared, and square of the current flowing through branch ij in the AC subgrid injected into node j at time t, respectively. $P_{in,t}^{ACPET}$, $P_{out,t}^{ACPET}$, $Q_{in,t}^{ACPET}$, $Q_{out,t}^{ACPET}$ are the active reactive power flowing into and out of the PET AC port.

DC part:

$$P_{j,t}^{DC} = \sum_{k\in\delta(j)} P_{jk,t}^{DC} - \sum_{i\in\pi(j)} \left(P_{ij,t}^{DC} + \tilde{I}_{ij,t}^{DC} r_{ij} \right) \tag{14}$$

$$\tilde{V}_{j,t}^{DC} = \tilde{V}_{i,t}^{DC} - 2r_{ij} P_{ij,t}^{DC} + r_{ij}^2 \tilde{I}_{ij,t}^{DC} \tag{15}$$

$$\left\| \begin{matrix} 2P_{ij,t}^{DC} \\ \tilde{I}_{ij,t}^{DC} - \tilde{V}_{j,t}^{DC} \end{matrix} \right\|_2 \le \tilde{I}_{ij,t}^{DC} - \tilde{V}_{j,t}^{DC} \tag{16}$$

$$P_{j,t}^{DC} = P_{j,t}^{WT} + P_{j,t}^{PV} + P_{in,t}^{DCPET} - P_{out,t}^{DCPET} - P_{j,t}^{DCLoad} \tag{17}$$

where B^{DC} and L^{DC} are the sets of DC subnet nodes and branches, respectively, and $P_{j,t}^{DC}$ is the active power injected into node j at time t of the DC subnet. $P_{ij,t}^{DC}$ is the active power flowing from i to j on DC branch ij; $\tilde{I}_{ij,t}^{DC}$ and $\tilde{V}_{j,t}^{DC}$ are the square of the current flowing through the ij branch from i to j and the square of the voltage at i in the DC

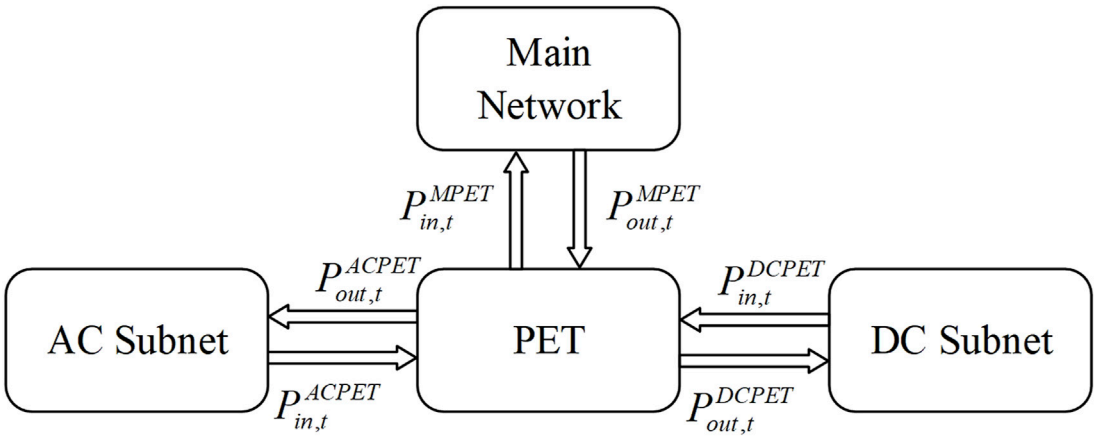

FIGURE 2
Schematic diagram of PET energy flow.

subnet, respectively; and $P_{in,t}^{DCPET}$ and $P_{out,t}^{DCPET}$ are the power flowing into and out of the PET DC port, respectively.

2.3.2 Operational constraints of distributed power generation

(1) Upper and lower limit constraints of micro turbine output:

$$\begin{cases} 0 \le P_{i,t}^{MT} \le P_i^{MTmax} \\ 0 \le Q_{i,t}^{MT} \le Q_i^{MTmax} \end{cases} \tag{18}$$

where P_i^{MTmax} and Q_i^{MTmax} are the maximum values of active and reactive power of the micro turbine, respectively. Because the step size selected in this model was 1 h, the regulation speed of the micro turbine was faster at this time scale, so the climbing constraint of the model was not considered.

(2) Wind turbine and photovoltaic output constraints:

$$0 \le P_{i,t}^{WT} \le \tilde{P}_{i,t}^{WT}, \forall t, \forall j \in B^{WTG} \tag{19}$$

$$0 \le P_{i,t}^{PV} \le \tilde{P}_{i,t}^{PV}, \forall t, \forall j \in B^{PV} \tag{20}$$

where $\tilde{P}_{i,t}^{WT}$ and $\tilde{P}_{i,t}^{PV}$ are the predicted wind turbine and PV outputs, respectively.

(3) Operational constraints of energy storage:

$$\begin{cases} 0 \le P_{i,t}^{ch} \le U_i(t) P^{ch}_{max} \\ 0 \le P_{i,t}^{dis} \le [1 - U_i(t)] P^{dis}_{max} \end{cases} \tag{21}$$

$$E_{i,t} = E_{i,t+1} - \eta P_{i,t}^{ch} + \frac{P_{i,t}^{dis}}{\eta} \tag{22}$$

$$E_i^{min} \le E_{i,t} \le E_i^{max} \tag{23}$$

where $P_{i,t}^{ch}$, $P_{i,t}^{dis}$ denote the charging and discharging power at node i at time t; P^{ch}_{max}, P^{dis}_{max} denote the maximum charging and discharging power of the energy storage device, respectively. $U_i(t)$ denotes the 0–1 correlation variable of the charging and discharging states at node i at time t, and 1 is charging and 0 is discharging. $E_{i,t}$, E_i^{max} denote the existing and maximum power stored in the energy storage device at node i at time t, respectively, and η denotes the charging and discharging efficiency of the energy storage device.

2.3.3 Operational constraints of power electronic transformers

In this study, we considered an AC/DC/AC-type PET with a DC section, which can be connected to multiple AC/DC distribution networks simultaneously because of its multi-port feature, and realize the power interaction function between each sub-network and the higher-level network through its AC/DC ports. Considering the limitations of PET, the amount of power interaction between each port was constrained.

Figure 2 shows a schematic diagram of the energy flow of the PET, where $P_{in,t}^{MPET}$ and $P_{out,t}^{MPET}$ are the active powers exchanged between the medium-voltage AC side port of the PET and the main network at moment t; $P_{in,t}^{ACPET}$ and $P_{out,t}^{ACPET}$ are the active powers exchanged between the low-voltage AC side of the PET and the AC distribution network at moment t; and $P_{in,t}^{DCPET}$ and $P_{out,t}^{DCPET}$ are the active powers exchanged between the low-voltage DC side of the PET and the DC distribution network at moment t (Zhang et al., 2017).

Letting the loss factor of PET be k_p and simplifying PET to a node (Li et al., 2018; Li et al., 2019; Li et al., 2021), we obtain:

$$P_{out,t}^{ACPET} + P_{out,t}^{DCPET} = k_p\left(P_{in,t}^{M} + P_{in,t}^{ACPET} + P_{in,t}^{DCPET}\right) \tag{24}$$

The capacity constraints of PET ports are:

$$\sqrt{\left(P_{in,t}^{MPET}\right)^2 + \left(Q_{in,t}^{MPET}\right)^2} \le S_{max}^{MPET} \tag{25}$$

$$\sqrt{\left(P_{out,t}^{MPET}\right)^2 + \left(Q_{out,t}^{MPET}\right)^2} \le S_{max}^{MPET} \tag{26}$$

$$\sqrt{\left(P_{out,t}^{ACPET}\right)^2 + \left(Q_{out,t}^{ACPET}\right)^2} \le S_{max}^{ACPET} \tag{27}$$

$$\sqrt{\left(P_{in,t}^{ACPET}\right)^2 + \left(Q_{in,t}^{ACPET}\right)^2} \le S_{max}^{ACPET} \tag{28}$$

$$P_{out,t}^{DCPET} \le P_{max}^{DCPET} \tag{29}$$

$$P_{in,t}^{DCPET} \le P_{max}^{DCPET} \tag{30}$$

Linearizing the non-linear term in the constraint so that it is transformed into a rotating cone constraint yields:

$$\left(P_{in,t}^{M}\right)^2+\left(Q_{in,t}^{M}\right)^2\le 2\frac{S_{max}^{MPET}}{\sqrt{2}}\frac{S_{max}^{MPET}}{\sqrt{2}} \tag{31}$$

$$\left(P_{out,t}^{M}\right)^2+\left(Q_{out,t}^{M}\right)^2\le 2\frac{S_{max}^{MPET}}{\sqrt{2}}\frac{S_{max}^{MPET}}{\sqrt{2}} \tag{32}$$

$$\left(P_{out,t}^{ACPET}\right)^2+\left(Q_{out,t}^{ACPET}\right)^2\le 2\frac{S_{max}^{ACPET}}{\sqrt{2}}\frac{S_{max}^{ACPET}}{\sqrt{2}} \tag{33}$$

$$\left(P_{in,t}^{ACPET}\right)^2+\left(Q_{in,t}^{ACPET}\right)^2\le 2\frac{S_{max}^{ACPET}}{\sqrt{2}}\frac{S_{max}^{ACPET}}{\sqrt{2}} \tag{34}$$

where S_{max}^{MPET}, S_{max}^{ACPET}, and P_{max}^{DCPET} are the power limits of the low-voltage AC and DC ports in the PET, respectively.

2.3.4 Uncertainty set of wind turbine, photovoltaic power output

Owing to the stochastic uncertainty of wind power and PV output, we considered the uncertainty set to characterize the uncertainty of the scenery output:

$$\begin{cases} u=\left[u_{i,t}^{WT},u_{i,t}^{PV}\right],t\in T \\ u_{i,t}^{WT}=\left[\hat{u}_{i,t}^{WT}-\Delta u_i^{WTmax},\hat{u}_{i,t}^{WT}+\Delta u_i^{WTmax}\right] \\ u_{i,t}^{PV}=\left[\hat{u}_{i,t}^{PV}-\Delta u_i^{PVmax},\hat{u}_{i,t}^{PV}+\Delta u_i^{PVmax}\right] \end{cases} \tag{35}$$

where $u_{i,t}^{WT}$, $u_{i,t}^{PV}$ are the actual wind and PV power, which are uncertainties; $\hat{u}_{i,t}^{WT}$, $\hat{u}_{i,t}^{PV}$ are the predicted values of wind and PV power; and Δu_i^{WTmax}, Δu_i^{PVmax} are the maximum deviation values allowed for wind and PV power, respectively.

To regulate the uncertainty of the model to control the conservativeness of the model, the time regulation parameters Γ_{WT}^{T}, Γ_{PV}^{T} and spatial regulation parameters Γ_{WT}^{S}, Γ_{PV}^{S} were introduced to represent the number of worst-case scenarios and wind turbines and photovoltaic units in the worst case simultaneously in one operating cycle, respectively. The specific expressions are as follows:

$$\begin{cases} u_{i,t}^{WT}=\hat{u}_{i,t}^{WT}-B_{i,t}^{WT}\Delta u_i^{WTmax} \\ u_{i,t}^{PV}=\hat{u}_{i,t}^{PV}-B_{i,t}^{PV}\Delta u_i^{PVmax} \\ \sum_{i=1}^{n}B_{i,t}^{WT}\le\Gamma_{WT}^{S} \\ \sum_{i=1}^{n}B_{i,t}^{PV}\le\Gamma_{PV}^{S} \\ \sum_{t=1}^{T}\sum_{i=1}^{n}B_{i,t}^{WT}\le\Gamma_{WT}^{T} \\ \sum_{t=1}^{T}\sum_{i=1}^{n}B_{i,t}^{PV}\le\Gamma_{PV}^{T} \end{cases} \tag{36}$$

where $B_{i,t}^{WT}$, $B_{i,t}^{PV}$ indicate whether the ith wind power and PV unit take the worst case at time t and are 0–1 variables.

3 Two-stage robust optimization model

As mentioned above, the optimization objective of the proposed model in this study was to minimize the cost of running one cycle, and the objective function can be expressed in the form of Eq. 1. Without considering the uncertainty of the PV of the wind turbine, the compact form of the objective function can be expressed as:

$$\begin{cases} \min\limits_{x,y}\ c^T y \\ s.t.\boldsymbol{D}y\ge\boldsymbol{d}\#(a) \\ \boldsymbol{K}y=0\#(b) \\ \boldsymbol{F}x+\boldsymbol{G}y\ge\boldsymbol{h}\#(c) \\ \boldsymbol{I_u}y=\hat{\boldsymbol{u}}\#(d) \\ \left\|\boldsymbol{M}y\right\|_2\le\boldsymbol{g}^T y\#(e) \end{cases} \tag{37}$$

where c is the column vector of coefficients corresponding to the objective function; $\boldsymbol{D}$, $\boldsymbol{K}$, $\boldsymbol{F}$, $\boldsymbol{G}$, $\boldsymbol{I_u}$, and $\boldsymbol{M}$ are the coefficient matrices of the various constraint equations; and $\boldsymbol{d}$, $\boldsymbol{h}$, and $\boldsymbol{g}^T$ are the column vectors of constants in the constraints. Equation (a) is the set of all inequality constraints known to be associated with **y** in the previous section; Equation (b) is the set of all equation constraints known to be associated with **y** in the previous section; Equation (c) is the set of all inequality constraints containing both **x** and **y**; Equation (d) is the set of all uncertainty constraints, which are represented by the predicted values of each uncertain outflow in the deterministic model; and Equation (e) is the set of all second-order cone constraints.

Where **x** and **y** are optimization variables, and their expressions are:

$$\begin{cases} x=[U_i(t)]^T \\ y=\left[P_{i,t}^{MT},P_{i,t}^{WT},P_{i,t}^{PV},P_{i,t}^{ch},P_{i,t}^{dis},P_{in,t}^{MPET},\right. \\ \left.P_{in,t}^{ACPET},P_{out,t}^{ACPET},P_{in,t}^{DCPET},P_{out,t}^{DCPET}\right]^T \end{cases} \tag{38}$$

When the uncertain output of wind and light is considered, a two-stage robust optimization approach can be used to find the scenario with the lowest cost of operating one cycle when the uncertain value of the scenery output is taken to the worst operating scenario with a preset uncertainty concentration, which is mathematically represented as follows:

$$\begin{cases} \min\limits_{x}\left\{\max\limits_{u\in U}\ \min\limits_{y\in\Omega(x,u)}\boldsymbol{c}^T y\right\} \\ st.\quad x=(x_1,x_2\cdot\cdot,x_{2T})^T \\ x_i\in\{0,1\},\forall i\in(1,2,\cdots,2\mathrm{T}) \end{cases} \tag{39}$$

where the outer layer is the first stage of the minimization problem with **x** as the optimization variable, and the inner layer is the second stage of the maximum minimization problem with **u** and **y** as the optimization variables. The first layer of the minimization problem was the objective function of this study, that is, the cost of running a cycle was minimized, and $\Omega(x,u)$ represents the feasible domain for a given set of **x**, **u**, **y**, whose expressions are as follows:

$$\Omega(x,u)=\begin{cases} y \\ \boldsymbol{D}y\ge\boldsymbol{d},\rightarrow\boldsymbol{\alpha} \\ \boldsymbol{K}y=0\rightarrow\boldsymbol{\beta} \\ \boldsymbol{F}x+\boldsymbol{G}y\ge\boldsymbol{h}\rightarrow\boldsymbol{\gamma} \\ \boldsymbol{I_u}y=\hat{\boldsymbol{u}}\rightarrow\boldsymbol{\delta} \\ \left\|\boldsymbol{M}y\right\|_2\le\boldsymbol{g}^T y\rightarrow\boldsymbol{\lambda},\boldsymbol{\mu} \end{cases} \tag{40}$$

where $\boldsymbol{\alpha}$, $\boldsymbol{\beta}$, $\boldsymbol{\gamma}$, $\boldsymbol{\delta}$, $\boldsymbol{\lambda}$, and $\boldsymbol{\mu}$ are pairwise vectors corresponding to each constraint matrix.

4 Model solving

To facilitate the solution, the above optimization model must be transformed into the form of a standard two-stage robust optimization

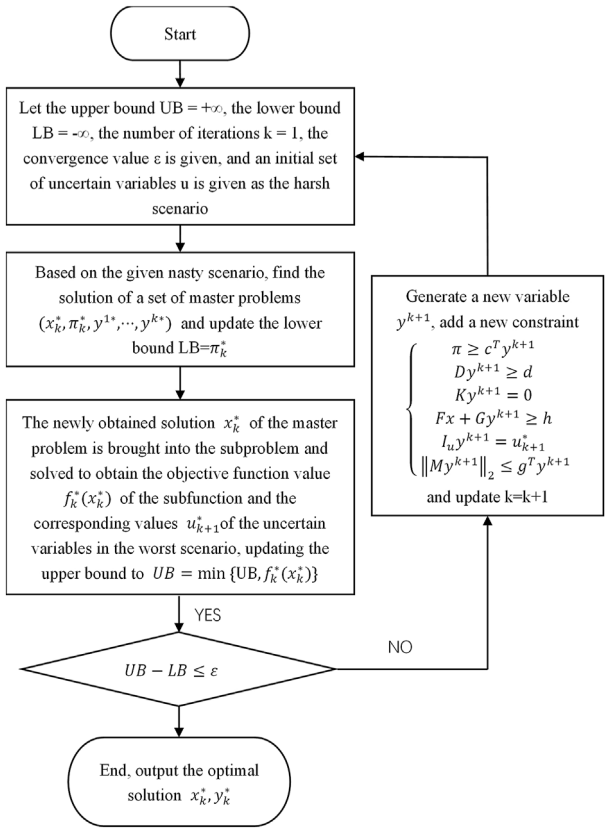

FIGURE 3
Algorithm flow chart.

model, which is a min-max-min multilayer optimization problem and is difficult to solve using general methods. In order to solve such problems, the commonly used methods are Benders decomposition method and Column and constraint generation (CCG) algorithm, and the CCG algorithm has the unique advantages of shorter computation time and fewer iterations compared with the Benders decomposition method, so the CCG algorithm is used to solve the two-stage robust optimization problem in this paper (Zeng and Zhao, 2013). The optimization problem was decomposed into a master problem and subproblem; the master problem min provided a lower bound for the subproblem max-min by calculation, whereas the subproblem provided a worst-case environment in the uncertainty set to provide an upper bound for the model, and then iterated the model several times so that the difference between the upper and lower bounds only decreased gradually. Finally, the result reached the preset convergence condition to obtain the desired optimization result. The specific process is as follows:

The main problem provides the lower bound for the model as:

$$\begin{cases} \min\limits_{x,y} \ \pi \\ st. \boldsymbol{\pi} \geq \boldsymbol{c}^T y_l \\ \boldsymbol{D} y_l \geq \boldsymbol{d} \# \\ \boldsymbol{K} y_l = 0 \# \\ \boldsymbol{F}x + \boldsymbol{G} y_l \geq \boldsymbol{h} \# \\ \boldsymbol{I_u} y_l = \boldsymbol{u_l^*} \# \\ \left\|\boldsymbol{M} y_l\right\|_2 \leq \boldsymbol{g}^T y_l \\ \forall \boldsymbol{l} \leq \boldsymbol{k} \end{cases} \tag{41}$$

where k is the number of current iterations, l is the number of historical iterations, y_l is the solution of the subproblem after l iterations, and $\boldsymbol{u_l^*}$ is the value of the uncertain variable u under the worst conditions obtained after the lth iteration.

The objective of the sub-problem was to derive the worst-case scenario with an objective function expressed as follows:

$$\max_{u \in U} \ \min_{y \in \Omega(x,u)} \boldsymbol{c}^T y \tag{42}$$

With (**x**,**u**) given, the subproblem can be viewed as a deterministic problem, and the equations of the subproblem are transformed into a dual form by the method mentioned above, thus transforming the min problem into a max problem for an easy solution, and the expression obtained is

$$\begin{cases} \max\limits_{u \in U, \alpha, \beta, \gamma, \delta, \varepsilon, \epsilon} \boldsymbol{d}^T \boldsymbol{\alpha} + (\boldsymbol{h} - \boldsymbol{F}x)^T \boldsymbol{\gamma} + u^T \boldsymbol{\delta} \\ \boldsymbol{D}^T \boldsymbol{\alpha} + K^T \boldsymbol{\beta} + \boldsymbol{G}^T \boldsymbol{\gamma} + \boldsymbol{I_u}^T \boldsymbol{\delta} \leq \boldsymbol{c} \\ \boldsymbol{\alpha} \geq 0, \boldsymbol{\gamma} \leq 0, \boldsymbol{\delta} \geq 0 \\ \|\boldsymbol{\lambda}\| \leq \boldsymbol{\mu} \end{cases} \tag{43}$$

The results obtained from the subproblem provide the upper bound for the whole model. The specific iteration process is shown in Figure 3.

5 Example analysis

5.1 Test platform and model parameters setting

To verify the correctness and effectiveness of this two-stage robust optimization method for hybrid AC-DC distribution networks with PET proposed in this study, the YALMIP toolbox and CPLEX and Gurobi solvers were used to solve the model. The hardware platform used was AMD Ryzen 7 4800 H 2.90 GHz; 16 GB RAM. The operating system used was Windows 10, and the software was R2017b. The structure of the algorithm used in this study is shown in Figure 4.

As shown in Figure 4, this study adopted a hybrid AC-DC distribution network model combined with two improved IEEE33 node models, where the red line indicates the AC part of the distribution network, and blue indicates the DC part. The PET connects the AC-DC part as well as the main network, and even plays the role of an energy hub. The voltage of the AC part was 12.66 kV and that of the DC part was 15 kV. The limitation range of the node voltage in the distribution network was $V_i \in [0.95, 1.05]$pu. The maximum value of the interaction power of the PET with the superior grid was $S_{max}^{MPET} = 12000\,kVA$, and the maximum value of the interaction power with the AC distribution network was $S_{max}^{ACPET} = 12000\,kVA$. The maximum value of the interactive power with the DC distribution network was $P_{max}^{DCPET} = 1000\,kV$, the loss coefficient of PET $k_p = 0.05$, and the iterative convergence accuracy of the CCG algorithm was set to $\varepsilon^c = 0.01$. The network was connected to energy storage devices ES and MT as controllable distributed power, and WT and PV as uncontrollable distributed power supplies; the specific distribution is shown in Figure 4. When the energy supply in the

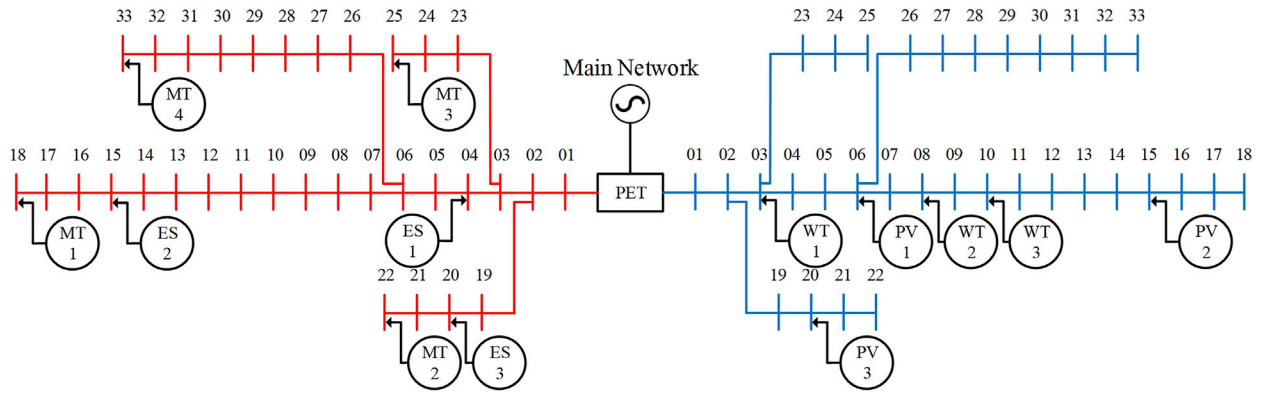

FIGURE 4
Structure diagram of AC/DC distribution network with PET.

TABLE 1 Output constraint of wind turbine.

No. Of wind turbine	Minimum output/kW	Maximum output power/kW
1	0	350
2	0	400
3	0	500

TABLE 2 Output constraint of photovoltaic.

No. Of wind photovoltaic	Minimum output/kW	Maximum output power/kW
1	0	300
2	0	350
3	0	500

TABLE 3 Parameters of micro turbine.

No. Of micro turbine	P_i^{MTmin}/kW	P_i^{MTmax}/kW	Q_i^{MTmin}/kW	Q_i^{MTmax}/kW	$c_1^{MT}/c_2^{MT}/c_3^{MT}$
1	125	350	75	210	0.10/30/0
2	80	300	48	180	0.12/29/0
3	150	375	90	225	0.14/22/0
4	50	250	30	150	0.11/25/0

AC or DC sub-network is insufficient, other sub-networks or higher-level grids can supply energy to them through PET. When there is a surplus of new energy in the DC sub-network, it can also be transmitted to the AC sub-network through PET, thus realizing peak reduction and valley filling in the distribution network to maximize economic benefits. The line parameters of the IEEE33 node system are detailed by (Kashem et al., 2000). The specific parameters of some devices are listed in the following Table 1, Table 2, Table 3, Table 4.

5.2 Analysis of simulation results

5.2.1 Results of running the two-stage robust optimization model

This example sets the spatial and temporal uncertainty regulation parameters $\Gamma_{WT}^{S} = \Gamma_{PV}^{S} = 2$ and $\Gamma_{WT}^{T} = \Gamma_{PV}^{T} = 12$. Figure 5 show the prediction curves for the wind turbine and photovoltaic outputs. The peak load was generally concentrated in the midday and evening hours, and the trough in the early

TABLE 4 Energy storage parameters.

No. Of energy storage	P_{min}^{ch} P_{min}^{dis}/kW	P_{max}^{ch} P_{max}^{dis}/kW	E_i^{min}/kW·h	E_i^{max}/kW·h	η
1	0	300	0	2000	0.95
2	0	300	0	2000	0.95
3	0	300	0	2000	0.95

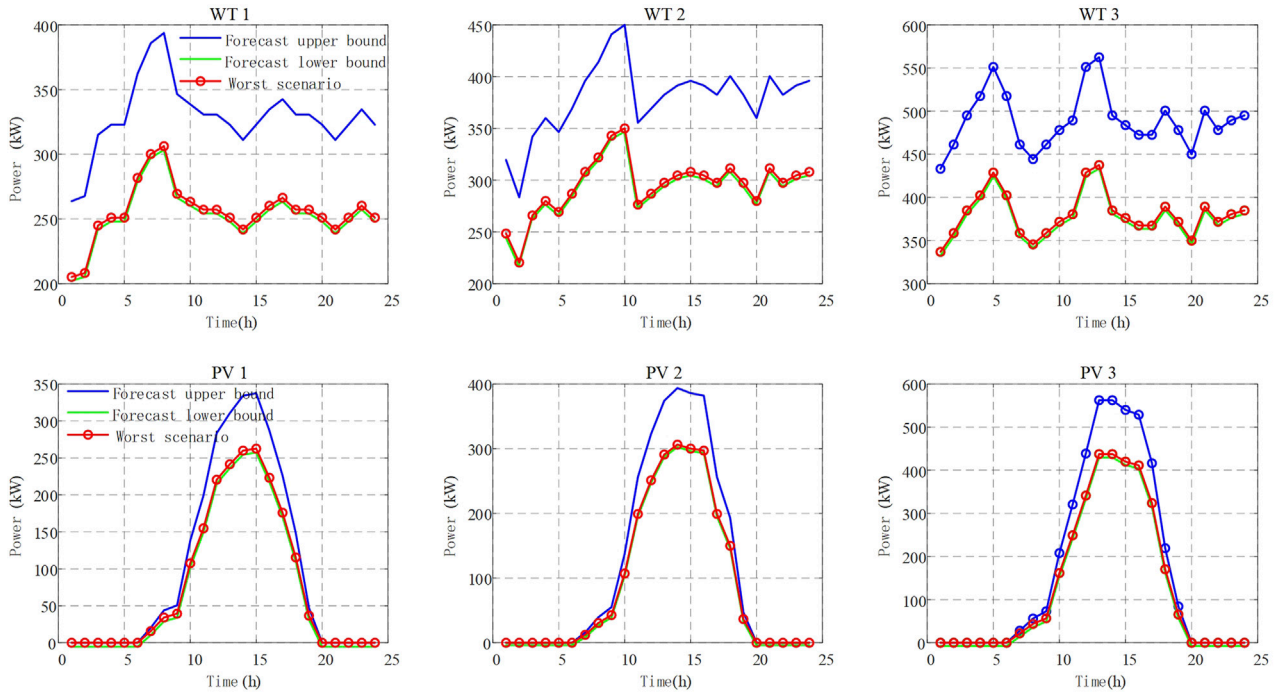

FIGURE 5
Output prediction curve of wind turbine and photovoltaic.

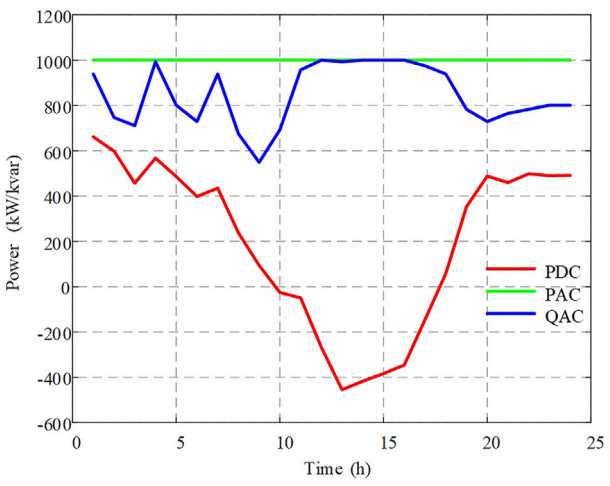

FIGURE 6
AC/DC port power of PET.

morning to morning hours. PV generated the most power at noon and hardly any at night, so wind power, PV, and MT must be combined to provide the power required by the load, with PET playing the role of energy router. Figure 6 and Figure 7 show the power output curves of the PET AC and DC ports and the power purchased by PET from the main grid, respectively. Figure 6 shows that during the time of high PV power generation around noon, the energy mainly flowed from the DC to the AC port, and the power purchased from the main grid during this time decreased. This reduced the costs of power purchase and abandonment penalty owing to the new energy consumption, thus achieving cost saving and new energy consumption. When there was no PV power at night, such as a DC subgrid power shortage, energy flowed from the AC to the DC port to ensure that the power was supplied to the load.

Comparing Figure 5 and Figure 8, the turbine generation was higher during the 5–10-h period, reducing the micro turbine generation at this time, thus reducing the system generation cost. Additionally, the dissipation of excess wind power reduced the

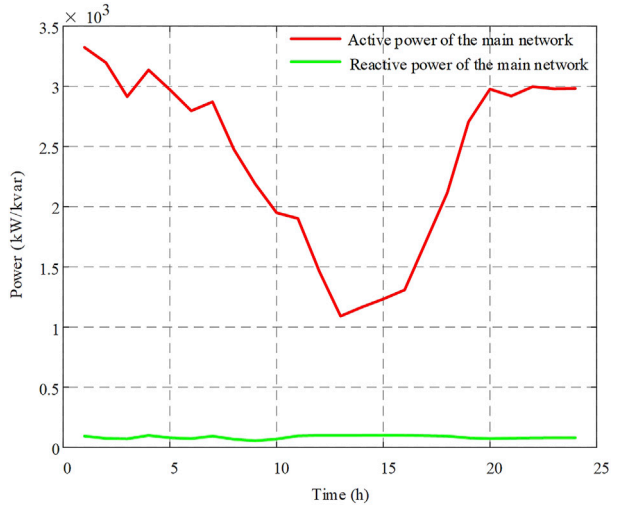

FIGURE 7
Purchased power to the main grid.

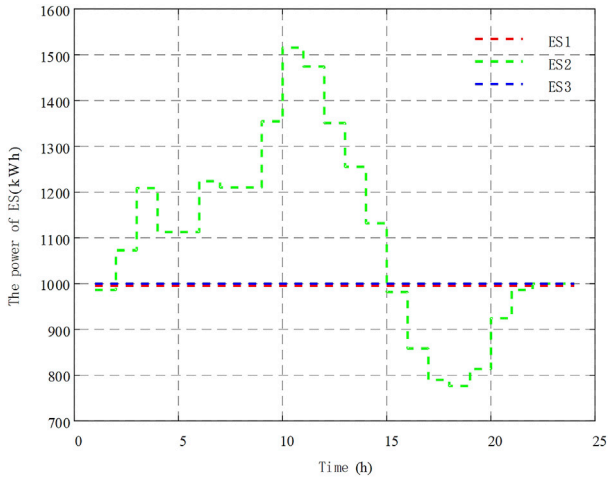

FIGURE 9
Energy storage curve.

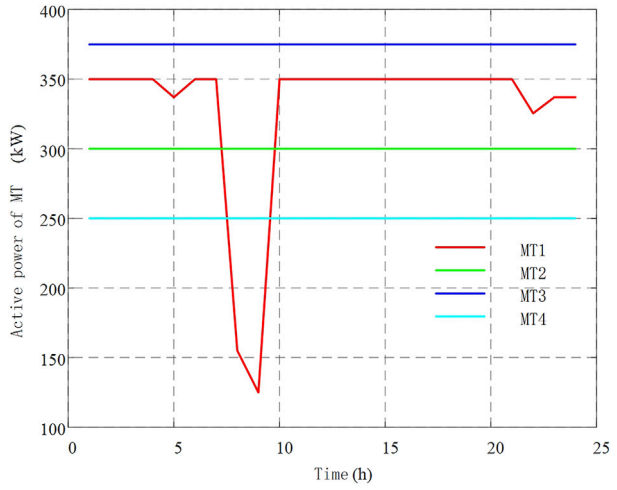

FIGURE 8
Power curve of micro turbine.

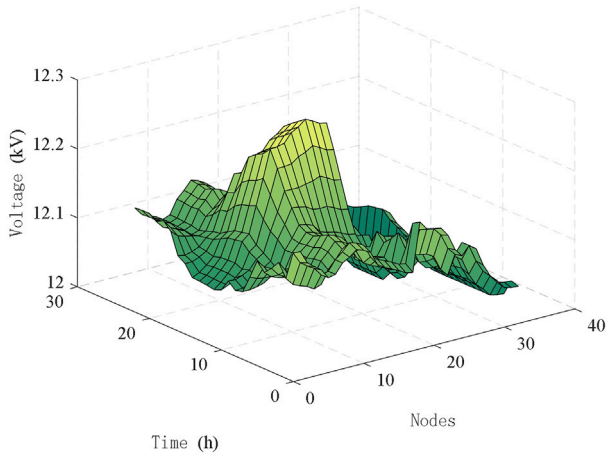

FIGURE 10
Voltage curve of DC section.

cost of the wind abandonment penalty. Figure 9 shows the energy storage power curves. When the overall new energy generation of the system was too large, energy could be stored to convert the power to the AC subnetwork through PET and store the excess energy in the storage device to reduce the cost of wind and light abandonment. In addition, when the overall system power was insufficient, it could also be discharged through energy storage to reduce power purchase and generation. When the system as a whole was short of power or when the cost of purchasing power from the higher grid was lower than the cost of generating power, power could be purchased from the higher grid through the PET interaction port with the higher grid to meet the system's power demand.

Figure 10 shows the voltage curve of the DC part of this model. Due the limitation of the number of graphs, we did not depict the nodal voltage curve of AC part as the AC part is similar to the DC part.

5.2.2 Comparison with deterministic and stochastic optimization models

The deterministic and stochastic optimization models were compared with the two-stage optimization model proposed in this study. By comparing the cost of operating the distribution network for one cycle under these conditions, the superiority of the models was verified. Furthermore, the impact of the uncertainty parameters on the conservative model was analyzed by comparing the cost of the models under different uncertainty parameters and number of iterations. The model

TABLE 5 Influence of uncertain parameters on results.

Optimization methods	Γ_{WT}^{T}、Γ_{PV}^{T}	Γ_{WT}^{S}、Γ_{PV}^{S}	Cost	Number of iterations
Two-stage robust optimization method	12	2	1518673.24	5
	12	3	1545173.23	5
	6	2	1429048.22	7
	6	1	1402673.23	8
	18	3	1624073.23	5
Deterministic optimization methods	0	0	842425	—
Stochastic optimization method	-	—	1269971.12	—

used in this study can be set with different uncertainty adjustment parameters for different DGs; however, for the convenience of presentation, the uncertainty adjustment parameters were the same for each DG in this study.

To verify the control effect of the uncertainty regulation parameter on the conservative type of model, several comparison tests were experimentally designed, as shown in Table 5, showing that the uncertain model was equivalent to the deterministic model when the uncertainty parameter was equal to 0. As the spatial and temporal uncertainty regulation parameters of the system increased, the number of units obtaining the worst case simultaneously and the total number of units that obtained the worst case in one operation cycle also increased. The uncertainty of the system also increased, increasing the cost of the model in one operation cycle, but the computation time and number of iterations decreased. This indicates that the more uncertainty the model considered, the worse the simulated operating conditions were, and the more conservative and costly the model was. Although the deterministic model had the lowest operating cost, it was not robust and, thus, could not cope with the uncertainty of new energy sources. The two-stage robust optimization model used in this study had a higher cost compared with the deterministic model, but it was robust because it considered the uncertainty of new energy. The larger the uncertainty parameter was, the more robust the model was, and the more it could cope with the uncertainty.

Compared with the stochastic optimization model commonly used in the literature mentioned previously, the cost of running one cycle of the stochastic optimization model was between that of the two-stage robust optimization and deterministic models. However, because the stochastic optimization model requires too many scenarios to be considered in the calculation, the calculation speed of the algorithm is slower, making its calculation time longer than that of the model used in this study. Additionally, the stochastic optimization model cannot guarantee the conservativeness of the calculation results, and the results have a certain probability of crossing the limit, which is not conducive to the safe power supply of the distribution network. The model used in this study can control the parameters of time and space uncertainty adjustment according to the actual situation to control the number of DGs of bad scenes in one cycle simultaneously, thus controlling the cost of running the model for one cycle. Therefore, the model used in this study is considered to have higher controllability and robustness when dealing with the actual problem.

5.2.3 Costs for different power supply configurations

The spatial uncertainty regulation parameter $\Gamma_{WT}^{S} = \Gamma_{PV}^{S} = 2$ and the temporal uncertainty regulation parameter $\Gamma_{WT}^{T} = \Gamma_{PV}^{T} = 12$. The cost is f = 1,518,673.24 when the power source in the optimization model contains both MT, ES and distributed new energy, which is used as a control group to compare and analyze the change of cost in other cases. When the model contains only MT and distributed new energy, the cost is f = 1759756.56. The reason for the increase in cost is that when there is no ES, it is not possible to reduce the peak and fill the valley, which makes the cost of wind and light abandonment penalty higher, and when the new energy output decreases, there is no energy storage to discharge, so we can only rely on MT power generation and purchase power from the upper grid, which increases the cost. When the model contains only MT, the overall power output of the system is too small to complete the power balance, resulting in the model cannot be iterated, and the cost results cannot be obtained.

6 Conclusion

This study established an optimal operation model of hybrid AC-DC distribution network with PET based on a two-stage robust optimization method, which considered the uncertainty of scenic power generation by using two-stage robust optimization. Based on ensuring the safety and reliability of the distribution network, the AC-DC part of the distribution network and super grid are connected by PET to improve the utilization rate of new energy and ensure the safe and economic operation of the distribution network. A comparison of the proposed model with deterministic and stochastic optimization models indicates that the model is more robust and can regulate the uncertainty of the system through the uncertainty parameters. However, the method used in this paper has the disadvantage of high cost, the next step will be to consider how to

model the uncertainty of renewable energy output in an AC-DC distribution network containing PET using a data-driven approach with a large amount of historical renewable energy data.

Data availability statement

The raw data supporting the conclusion of this article will be made available by the authors, without undue reservation.

Author contributions

The HD wrote the original draft. MW and ZT provided the supervision, review, and editing of the draft. All authors contributed to the article and approved the submitted version.

Funding

National Natural Science Foundation of China (61872230).

Acknowledgments

We would like to thank Editage (www.editage.cn) for English language editing.

Conflict of interest

The authors declare that the research was conducted in the absence of any commercial or financial relationships that could be construed as a potential conflict of interest.

Publisher's note

All claims expressed in this article are solely those of the authors and do not necessarily represent those of their affiliated organizations, or those of the publisher, the editors and the reviewers. Any product that may be evaluated in this article, or claim that may be made by its manufacturer, is not guaranteed or endorsed by the publisher.

References

Fu, Y., Zhang, Z. Q., and Li, Z. K. (2019). Research on reactive power voltage control strategy for hybrid AC/DC distribution network based on two-stage robust optimization model [J]. *Proc. CSEE* 39 (16), 4764–4774+4978. doi:10.13334/j.0258-8013.pcsee.180940

Guo, S. Q., Mu, Y. F., Chen, N. S., Pu, T. J., Yuan, X. D., and Li, Q. (2019). Day-ahead optimal scheduling of AC/DC hybrid distributed energy system with power electronic transformer [J]. *Adv. Technol. Electr. Eng. Energy* 38 (02), 44–51. doi:10.12067/ATEEE1806018

Kashem, M. A., Ganapathy, V., Jasmon, G. B., and Buhari, M. I. (2000). "A novel method for loss minimization in distribution networks. Electric Utility Deregulation and Restructuring and Power Technologies," in Proceedings. DRPT 2000. International Conference on. IEEE Xplore.

Lavaei, J., and Low, S. H. (2012). Zero duality gap in optimal power flow problem. *IEEE Trans. Power Syst. A Publ. Power Eng. Soc.* 27 (1), 92–107. doi:10.1109/TPWRS.2011.2160974

Li, K., Zhao, Z. M., Yuan, L. Q., Gao, C. Y., Wen, W. S., and You, X. J. (2021). Overview on research of multi-port power electronic transformer oriented for AC/DC hybrid distribution grid [J]. *High. Volt. Eng.* 47 (04), 1233–1250. doi:10.13336/j.1003-6520.hve.20201250

Li, S. C., Ling, Y. S., Pang, T. Y., and Zhang, H. Y. (2018). Research on power electronic transformer based on AC/DC and DC/AC two level structure [J]. *Electr. Energy Manag. Technol.* 543 (06), 7–10. doi:10.16628/j.cnki.2095-8188.2018.06.002,No.

Li, X. Y., Hu, Y., Zhu, B. T., and Geng, Q. (2019). Optimal configuration of hybrid AC/DC distribution network with power electronic transformer based on genetic algorithm. *J. Water Resour. Power* 37 (09), 192–196.

Liao, H. T., Huang, Y. H., Shi, Y. Z., and Chen, J. (2020). A Bi-level two-stage robust optimal operation strategy for AC and DC distribution network with photovoltaic and energy storage [J]. *Electr. Power Constr.* 41 (03), 110–118.

Liu, C., and Zhi, K. L. (2017). Hybrid cascaded power electronics transformer topology and control scheme [J]. *Power Syst. Technol.* 41 (02), 596–603. doi:10.13335/j.1000-3673.pst.2016.0942

Liu, Y. X., Guo, L., and Wang, C. S. (2018). Economic dispatch of microgrid based on two stage robust optimization [J]. *Proc. CSEE* 38 (14), 4013–4022+4307. doi:10.13334/j.0258-8013.pcsee.170500

Pu, T., J., Li, Y., Chen, N. S., Sun, Y. Y., Mu, Y. F., Dong, L., et al. (2018). Key technology and research framework for optimal operation control of hybrid AC/DC system based on power electronic transformer. *J. Power Syst. Technol.* 42 (09), 2752–2759. doi:10.13335/j.1000-3673.pst.2018.0730

Wang, Y., Zheng, Z. D., and Li, Y. D. (2017). Review of topology and control application of medium and high voltage power electronic transformer [J]. *Adv. Technol. Electr. Eng. Energy* 36 (05), 1–10.

Xu, C. B., Yang, X. D., Zhang, Y. B., Zhang, K. Y., Wang, X. Z., and Tang, M. (2021). Stochastic operation optimization method for active distribution networks with soft open point considering risk management and control [J]. *Automation Electr. Power Syst.* 45 (11), 68–76. doi:10.7500/AEPS20200331004

Yi, W. F., and Wang, X. (2021). Research on power electronic transformer based day-ahead economic operation strategy of AC/DC hybrid distribution network [J]. *Mod. Electr. Power* 38 (03), 339–345. doi:10.19725/j.cnki.1007-2322.2020.0393

Zeng, B., and Zhao, L. (2013). Solving two-stage robust optimization problems using a column-and-constraint generation method. *Operations Res. Lett.* 41 (5), 457–461. doi:10.1016/j.orl.2013.05.003

Zhang, T., Mu, Y. F., Jia, H. J., Wang, Y. X., and Pu, T. J. (2022). Stochastic operation optimization for AC/DC distribution network with power electronic transformer. *J. Power Syst. Technol.* 46 (03), 860–869. doi:10.13335/j.1000-3673.pst.2021.0536

Zhang, X. L., Zhou, H., Xiao, Z. H., Zhang, W., and Wu, D. (2017). Power electronic transformer applied to optimization of reactive power in active distribution system [J]. *Power Syst. Prot. Control* 45 (04), 80–85. doi:10.7667/PSPC160321

Zhang, X., Yao, L., Chen, C., Fang, R. S., and Lin, J. K. (2022). A novel two-stage robust model for Co-optimization of reconfiguration and reactive power in AC/DC hybrid distribution network [J]. *Power Syst. Technol.* 46 (03), 1149–1162. doi:10.13335/j.1000-3673.pst.2020.1870

Zhong, L., Gao, H. J., Yang, Y. H., Liu, Y. B., and Liu, J. Y. (2022). Load peak shaving operation management and control strategy of AC/DC hybrid distribution network based on two-stage robust game model [J]. *Proc. CSEE* 42 (15), 5550–5565. doi:10.13334/j.0258-8013.pcsee.210628